AD-A080 549 SRI INTERNATIONAL MENLO PARK CA F/G 4/1
ON THE SPATIAL RELATIONSHIP OF 1-METER EQUATORIAL SPREAD-F IRRE--ETC(U)
APR 79 R T TSUNODA DNA001-79-C-0153

UNCLASSIFIED DNA-4935T NL

| OF |
AD
A080549

END
DATE FILMED
3 -80
DDC

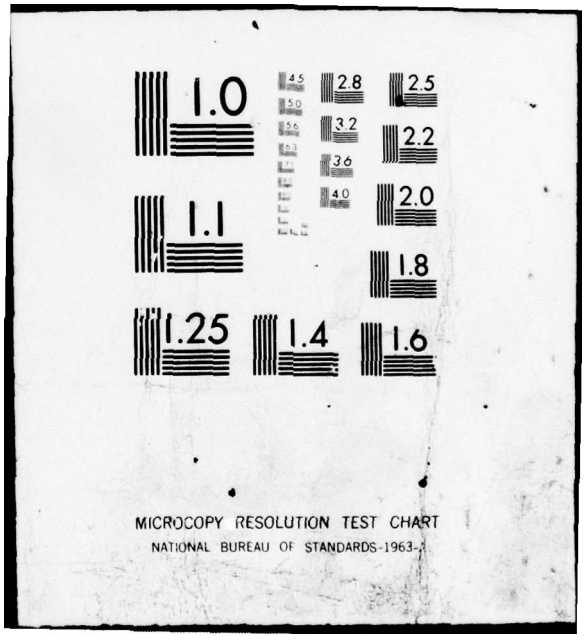
1.0
1.1
1.25
1.4
1.6
1.8
2.0
2.2
2.5
2.8
3.2
3.6
4.0
4.5
5.0
5.6
MICROCOPY RESOLUTION TEST CHART
NATIONAL BUREAU OF STANDARDS-1963-A

DNA 4935T

ON THE SPATIAL RELATIONSHIP OF 1-METER EQUATORIAL SPREAD-F IRREGULARITIES AND PLASMA BUBBLES

Roland T. Tsunoda
SRI International
333 Ravenswood Avenue
Menlo Park, California 94025

1 April 1979

Topical Report 2 for Period 15 February 1979—1 April 1979

CONTRACT No. DNA 001-79-C-0153

APPROVED FOR PUBLIC RELEASE;
DISTRIBUTION UNLIMITED.

THIS WORK SPONSORED BY THE DEFENSE NUCLEAR AGENCY
UNDER RDT&E RMSS CODE B322079462 I25AAXHX64009 H2590D.

Prepared for
Director
DEFENSE NUCLEAR AGENCY
Washington, D. C. 20305

Destroy this report when it is no longer needed. Do not return to sender.

PLEASE NOTIFY THE DEFENSE NUCLEAR AGENCY, ATTN: STTI, WASHINGTON, D.C. 20305, IF YOUR ADDRESS IS INCORRECT, IF YOU WISH TO BE DELETED FROM THE DISTRIBUTION LIST, OR IF THE ADDRESSEE IS NO LONGER EMPLOYED BY YOUR ORGANIZATION.

UNCLASSIFIED

SECURITY CLASSIFICATION OF THIS PAGE (When Data Entered)

REPORT DOCUMENTATION PAGE

READ INSTRUCTIONS BEFORE COMPLETING FORM

1. REPORT NUMBER: DNA 4935T

2. GOVT ACCESSION NO.:

3. RECIPIENT'S CATALOG NUMBER: n/a

4. TITLE (and Subtitle): ON THE SPATIAL RELATIONSHIP OF 1-METER EQUATORIAL SPREAD-F IRREGULARITIES AND PLASMA BUBBLES

5. TYPE OF REPORT & PERIOD COVERED: Topical Report 2. [redacted] 15 Feb [redacted]—1 Apr 79

6. PERFORMING ORG. REPORT NUMBER: SRI Project 8164

7. AUTHOR(s): Roland T. Tsunoda

8. CONTRACT OR GRANT NUMBER(s): Contract DNA001-79-C-0153

9. PERFORMING ORGANIZATION NAME AND ADDRESS:
SRI International
333 Ravenswood Avenue
Menlo Park, California 94025

10. PROGRAM ELEMENT, PROJECT, TASK AREA & WORK UNIT NUMBERS: Subtask I25AAXHX640-09

11. CONTROLLING OFFICE NAME AND ADDRESS:
Director
Defense Nuclear Agency
Washington, D.C. 20305

12. REPORT DATE: 1 Apr [redacted]79

13. NUMBER OF PAGES: 32

14. MONITORING AGENCY NAME & ADDRESS (if different from Controlling Office):

15. SECURITY CLASS (of this report): UNCLASSIFIED

15a. DECLASSIFICATION/DOWNGRADING SCHEDULE:

16. DISTRIBUTION STATEMENT (of this Report)

Approved for public release; distribution unlimited.

17. DISTRIBUTION STATEMENT (of the abstract entered in Block 20, if different from Report)

18 DNA, SBIE 19 4935T, AD-E300658

18. SUPPLEMENTARY NOTES

This work sponsored by the Defense Nuclear Agency under RDT&E RMSS Code B322079462 I25AAXHX64009 H2590D.

19. KEY WORDS (Continue on reverse side if necessary and identify by block number)

Equatorial spread F
Plasma bubbles
Ionospheric irregularities
Incoherent scatter

20. ABSTRACT (Continue on reverse side if necessary and identify by block number)

A radar experiment was conducted on 18 August 1978 at Kwajalein Atoll, Marshall Islands, to investigate the spatial relationship of 1-m equatorial spread-F irregularities to plasma bubbles (localized depletions in F-layer plasma density). East-west scans were made with ALTAIR, an incoherent-scatter radar, to spatially map (1) the backscatter produced by field-aligned irregularities, and (2) the electron-density distribution of the background F layer. Plasma bubbles were spatially mapped for the first time with an incoherent-

DD FORM 1 JAN 73 1473 EDITION OF 1 NOV 65 IS OBSOLETE

UNCLASSIFIED

SECURITY CLASSIFICATION OF THIS PAGE (When Data Entered)

410 281

(cont)

scatter radar. By assuming invariance along the magnetic field lines (over distances of less than 100 km), we show that 1-m field-aligned irregularities are directly related to plasma bubbles.

PREFACE

The author would like to thank Dr. D. M. Towle for his approval and support of this experiment, and the ALTAIR staff for their quick response to experiment requirements that were given on short notice.

TABLE OF CONTENTS

PREFACE 1

LIST OF ILLUSTRATIONS 3

I INTRODUCTION 5

II THE EXPERIMENT 7

III RESULTS 11

IV DISCUSSION AND CONCLUSIONS 21

REFERENCES 23

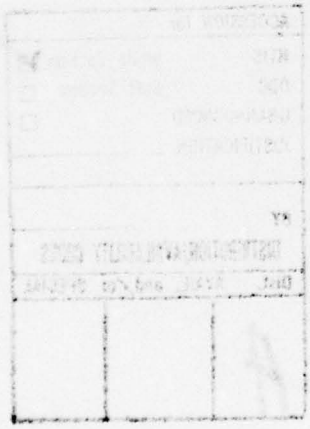

LIST OF ILLUSTRATIONS

1	Radar Scan Geometry Showing the Beam Positions of the Scan Made Perpendicular to the Magnetic Field and the Corresponding Off-Perpendicular Beam Positions	9
2	Backscatter-Intensity Contour Map Showing Two Backscatter Plumes Separated by a Region of No Backscatter	12
3	Electron-Density Profiles Obtained at Off-Perpendicular Beam Positions Corresponding to the Intense Backscatter Region Shown in Figure 2	13
4	A Comparison of Plume Backscatter Profiles (solid curves) and Corresponding Electron Density Profiles (dashed curves).	17
5	Electron-Density Profiles Obtained on 18 August 1978 with Radar Beam Fixed at 10° South (geomagnetic) of Vertical.	18
6	Electron-Density Profiles Obtained on 19 August 1978 with Radar Beam Fixed at 10° South (geomagnetic) of Vertical.	20

I INTRODUCTION

The disturbed, nighttime equatorial ionosphere has been found to contain two unique features, "plasma bubbles" and radar backscatter "plumes." Plasma bubbles are localized depletions in F-layer electron density which can be as much as three orders of magnitude below the ambient level (Hanson and Sanatani, 1973; McClure et al., 1977). Plasma bubbles are believed to extend throughout entire magnetic flux tubes with dimensions transverse to the geomagnetic field of up to a few hundred kilometers. Radar backscatter plumes are produced by meter-scale field-aligned irregularities (FAI) and extend from the bottomside into the topside of the F layer. Because plasma bubbles and radar plumes appear to possess similar characteristics, researchers have speculated that they are directly associated, if not spatially coincident (e.g., Woodman and La Hoz, 1976).

Although there have been several coordinated experiments (involving in-situ measurements of plasma depletions by rockets) whose results have suggested that a close relationship does exist (Kelley et al., 1976; Morse et al., 1977), the results have not been conclusive. Perhaps the most convincing evidence published thus far are those of Tsunoda and Towle (1979). They showed that large-scale (200 km in width) depletions in total electron content (TEC) were longitudinally coincident with radar backscatter plumes. However, because TEC in a range-integrated measurement, it was not possible to determine whether the regions of plasma depletion that produced the TEC depletions were spatially coincident with the backscatter plumes, or whether they were displaced in altitude from one another.

In this paper, we present spatial maps of plasma bubbles obtained with an incoherent-scatter (IS) radar. (Similar results have also been reported by Towle [1979]). Using ALTAIR, an IS radar located in the Kwajalein Atoll, Marshall Islands (Tsunoda et al., 1979), both plasma

bubbles and radar plumes were spatially mapped, sequentially in time. A comparison of the locations of plasma depletion and radar backscatter indicate that they are directly related.

II THE EXPERIMENT

The use of ALTAIR, a fully-steerable incoherent-scatter (IS) radar, for the spatial mapping of equatorial field-aligned irregularities (FAI) and the electron-density distribution of the background F layer was described by Tsunoda et al. (1979). Briefly, ALTAIR is located in the Kwajalein Atoll, Marshall Islands at a magnetic dip latitude of 4.3°N. The radar was operated for this experiment at 155.5 MHz, transmitting a 30-μs pulse through a 46-m paraboloid antenna having a 2.8° beamwidth.

In order to map plasma depletions using incoherent scatter, we must be able to suppress the contaminating effects of spread-F backscatter. Suppression of intense spread-F backscatter is accomplished by taking advantage of the field-aligned nature of the irregularities and the steerability of the ALTAIR antenna. Because of the strong magnetic aspect dependence of spread-F backscatter, IS measurements can be made with excellent suppression of spread-F backscatter by positioning the radar beam several degrees away from perpendicular aspect with the geomagnetic field.

A second consideration is the capability of the radar to resolve a plasma bubble. The smallest plasma bubble that can be resolved with ALTAIR is dependent on the range to the depletion. At 400 km, a typical distance from radar to a plasma bubble, the dimensions of the radar scattering volume are 4.5 x 20 x 20 km. Therefore, ALTAIR is capable of spatially mapping a plasma bubble that is larger than 4.5 km in range and 20 km in transverse distance. It is worth noting that the altitude extent of plasma depletions observed to date by rockets is on the order of 10 km, or less (Kelley et al., 1976; Morse et al., 1977). On the other hand, the horizontal dimensions of plasma bubbles appear to extend up to 200 km (McClure et al., 1977).

The experiment, conducted on 18 August 1978, consisted of operating ALTAIR in two discrete-scan modes, with one following immediately after

the other. The scan geometry for the two modes is shown in Figure 1. The coordinates are polar with radar azimuth measured from true north (top of the figure) in a clockwise direction. The first mode consisted of making a discrete, 25-position scan from west to east over a 72° angular sector, maintaining the radar beam perpendicular to the geomagnetic field at F-region altitudes. The odd-numbered beam positions for this scan mode are shown in Figure 1. The scan is seen to intersect the magnetic meridian at approximately 9° north of vertical. The radar beam was held fixed for about 15 seconds in each position, thus completing the scan in six minutes. With this type of scan, we were able to map the spatial distribution of radar backscatter plumes.

Upon completion of the first scan mode, the location of radar plumes was determined from real-time range-time-intensity (RTI) displays. Five off-perpendicular beam positions were then selected for the second scan mode which corresponded (when extrapolated along the magnetic field lines) to the vicinity of maximum backscatter strength within a radar plume. The five beam positions were selected from 25 preselected, off-perpendicular beam positions that corresponded to those in the first scan mode, as shown in Figure 1. Incoherent-scatter measurements were then recorded for one minute at each of those beam positions.

The off-perpendicular beam positions in Figure 1 (primed numbers) correspond to the beam positions in the first scan mode labeled with the same, but unprimed numbers. Note that the off-perpendicular beam positions are offset southward from the unprimed beam positions by about 13°. With this displacement, the first sidelobe (estimated to be approximately 6° away from boresight of the main beam) is kept well away from the contour of exact orthogonality with the magnetic field lines. Consequently, we believe that suppression of backscatter from spread-F irregularities is well below -36 dB, the (two-way) gain of the first sidelobe relative to the main lobe. In fact, the suppression is probably closer to -50 dB, as indicated by the data presented in the following section.

In order to assure this level of suppression, we sacrificed near-spatially-coincident measurements and introduced the assumption that

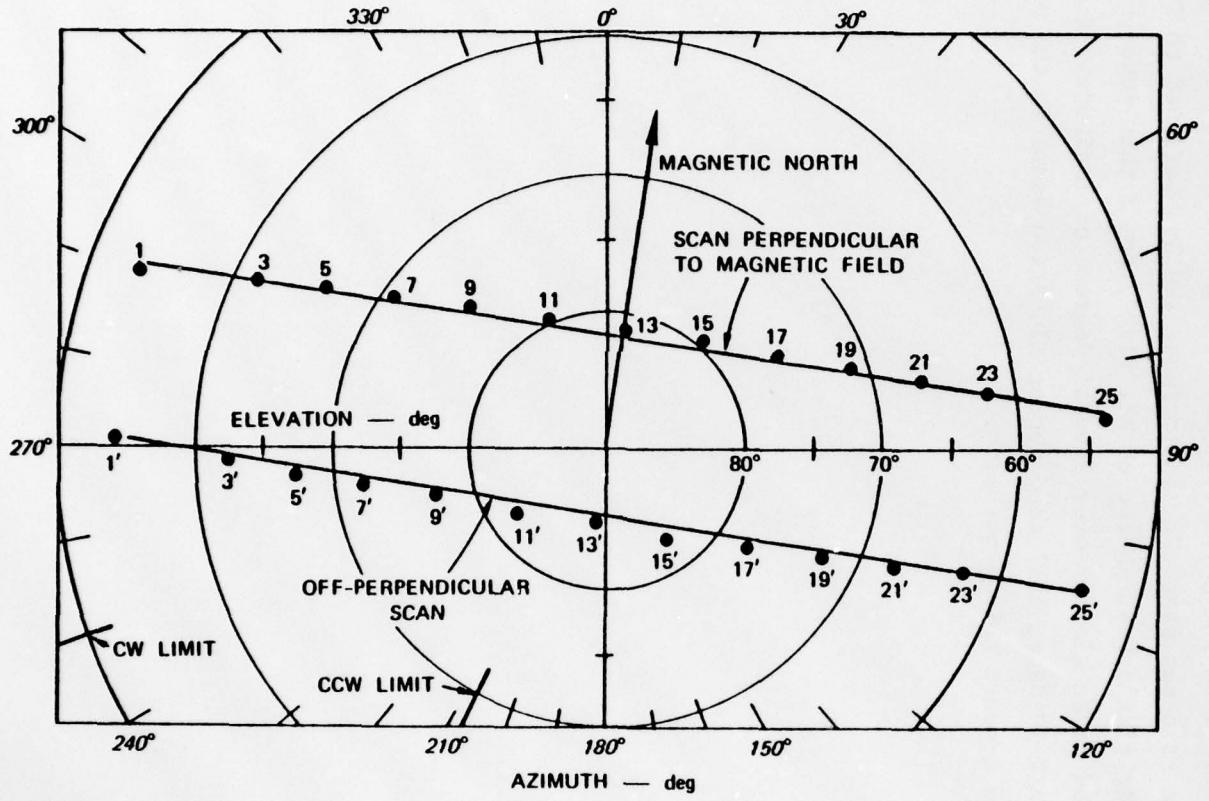

FIGURE 1 RADAR SCAN GEOMETRY SHOWING THE BEAM POSITIONS OF THE SCAN MADE PERPENDICULAR TO THE MAGNETIC FIELD AND THE CORRESPONDING OFF-PERPENDICULAR BEAM POSITIONS

both 1-m FAI features and plasma depletions map along magnetic field lines. This assumption is considered to be very reasonable since 13° angular separation at 400-km range corresponds to a spatial separation of 90 km, or less than a degree of latitude. Equatorial spread-F phenomena are known to occur over ±20° in latitude and are believed to involve entire magnetic flux tubes. Morse et al. (1977) found that ionospheric features tended to be similar over several degrees of latitude. Unpublished ALTAIR IS data, collected during elevation scans in the magnetic meridian, also support this hypothesis.

III RESULTS

The spatial distribution of backscatter from 1-m FAI obtained from the first scan mode is shown in Figure 2. The contours of constant backscatter strength (corrected for range dependence) which are plotted in 10-dB steps, are referenced to the IS signal strength associated with an electron density of 10^6 el/cm^3. In other words, the 0-dB contour corresponds in signal strength to incoherent backscatter that would be obtained from an electron density of 10^6 el/cm^3. The 10-dB contour corresponds to an equivalent electron density of 10^7 el/cm^3, and so on.

Two backscatter plumes are seen in Figure 2, separated by a region of no backscatter. The larger plume in the west half of the contour map is seen to be connected to backscatter from the bottomside F layer and extends upward (and westward) to altitudes near 700 km. Both radar plumes are typical of those seen with ALTAIR on very disturbed nights (e.g., Tsunoda and Towle, 1979) and similar to those observed at 50 MHz with the Jicamarca IS radar (Woodman and La Hoz, 1976).

The region of strongest backscatter (greater than 30 dB) occurred in beam positions 5 through 8. Having examined the RTI display (corresponding to Figure 2) in real time, we estimated the locations of strongest backscatter and selected off-perpendicular beam positions 6′ through 10′ for IS measurements.

The electron density profiles obtained from the five off-perpendicular beam positions are shown in Figure 3. Each profile is labeled with its time of measurement, and shaded in regions where the electron density is greater than 10^5 el/cm^3. Extreme care should be taken in the interpretation of the structure seen in the profiles, particularly since the IS data were noisy above 600 km. Because of poor signal-to-noise ratio, the variations in electron density above 600 km should not be considered to be real. Together with the profiles are shown vertical black bars which represent the altitude extent over which spread-F backscatter was observed.

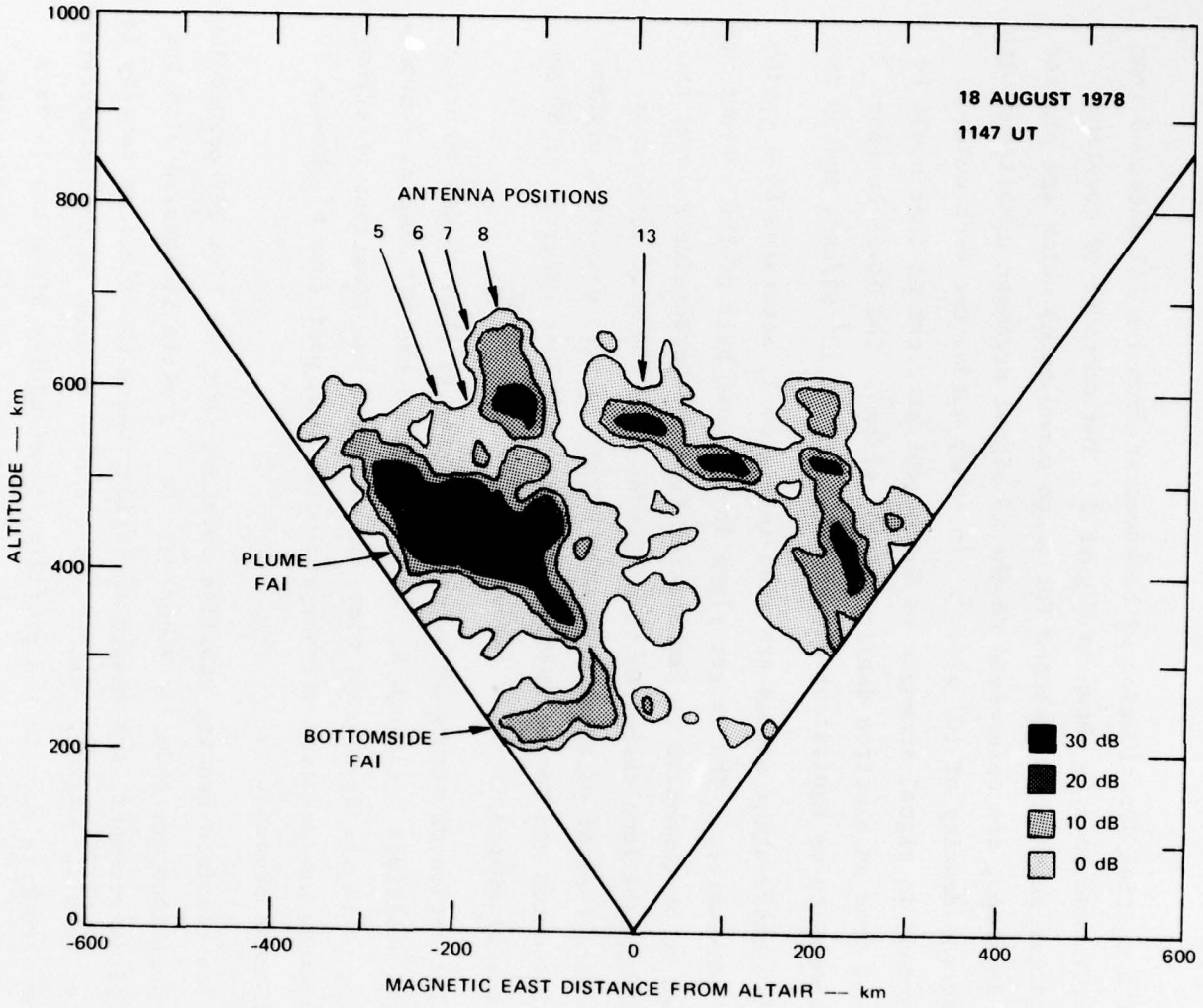

FIGURE 2 BACKSCATTER-INTENSITY CONTOUR MAP SHOWING TWO BACKSCATTER PLUMES SEPARATED BY A REGION OF NO BACKSCATTER

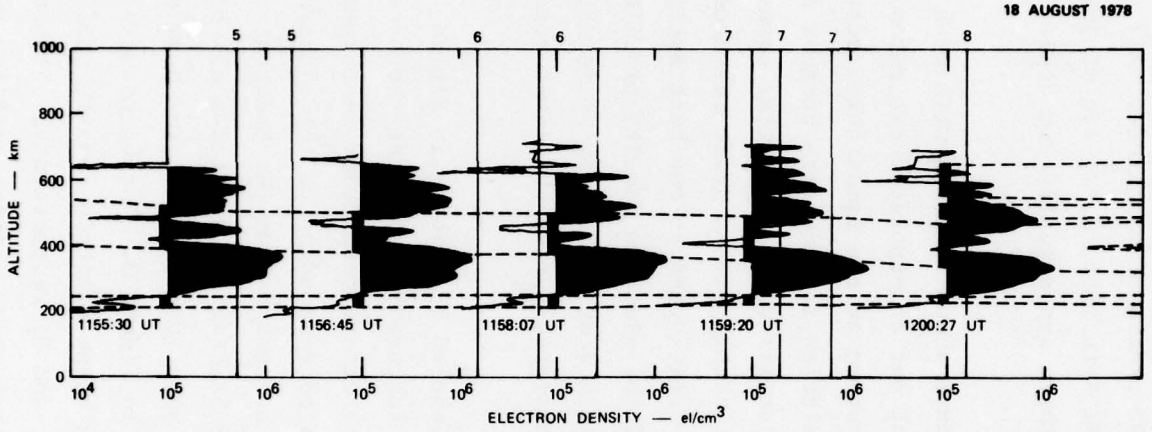

FIGURE 3 ELECTRON-DENSITY PROFILES OBTAINED AT OFF-PERPENDICULAR BEAM POSITIONS CORRESPONDING TO THE INTENSE BACKSCATTER REGION SHOWN IN FIGURE 2

Examining the electron density profiles, we find that all of the profiles are characterized by a major depletion located near 450 km altitude, very close to the peak of the F layer. The plasma depletion extends over 100 km in altitude with a percentage depletion that, in some cases, approaches two orders of magnitude. All of the depletions also have similar internal structure, i.e., two minima in electron density, suggesting that perhaps there are actually two depletions contiguous in altitude.

The black vertical bars shown together with each electron density profile actually represent our interpolated estimates of where spread-F backscatter must have occurred at the times the electron density measurements were made. Interpolation is necessary because of an eastward, bulk-plasma drift that prevails in the nighttime equatorial ionosphere (Woodman, 1972). Without actual plasma drift measurements, we used a nominal 100 m/s eastward drift speed as our best estimate. Then using the horizontal spacing of the electron density profiles in Figure 3 as the relative spacing between beam positions, we interpolated the locations of spread-F backscatter measured during the first scan, made perpendicular to the magnetic field.

The vertical lines labeled by numbers in Figure 3 show the relative locations of backscatter features measured at those beam positions, at times corresponding to the off-perpendicular measurements. For example, the backscatter altitudes corresponding to the electron density profile taken at 1155:30 UT were estimated from the backscatter in beam positions 4 (not shown) and 5. The backscatter altitudes associated with the profile taken at 1156:45 UT were interpolated from beam positions 5 and 6 that bracket the profile in Figure 3. The backscatter altitudes associated with the remaining three electron density profiles were estimated from beam positions 6, 7, and 8, respectively. Except for the backscatter corresponding to the last electron density profile, the interpolation was not critical in placing the backscatter regions.

In all cases, we see that backscatter is associated with (1) the bottomside F layer, and (2) the plasma-depleted region. The only other backscatter that was observed were those found in the topside layer at

1200 UT. As shown, the spatial coincidence of radar backscatter and plasma depletions is excellent. The altitude extent of backscatter is seen to be comparable to the altitude extent of the plasma depletion. The fact that they both occur at similar altitudes and have comparable thicknesses (in altitude) is perhaps the most convincing evidence that radar backscatter and plasma bubbles are directly related.

If we compare the altitudes of the plasma depletions found in each profile, we find that the depletions occur at lower altitudes as we look further eastward. Since the five beam positions are contiguous, the systematic variation in depletion altitude can be interpreted as evidence of a single, slab-like depletion in electron density that is tilted. Ignoring any vertical transport that might be associated with the plasma depletion, such as an upward bubble rise-velocity (e.g., Ossakow and Chaturvedi, 1978), or a bulk downward movement of the entire F layer, we find that the slab-like depletion is tilted at an apparent angle of 60° west of vertical.

Referring back to Figure 2, we note that the tilt found in the plasma depletion is in the same sense as the tilt found in the 20 dB contour of corresponding backscatter region. This comparison is reasonable because the location and altitude extent of the 20 dB contour are comparable to that of the plasma depletion. However, a quantitative comparison of tilt angles is difficult. (For example, the tilt of the 30 dB contour is completely different from that of the 20 dB contour.)

The exact spatial relationship between the two phenomena is less clear. If we extrapolate from the region of spread-F backscatter along a magnetic flux tube to the location of IS measurement, we must shift the backscatter region upward in altitude by about 15 km. We must also account for any vertical transport that might have occurred between the time of spread-F backscatter measurements and the time of IS measurements.

For a more detailed comparison between plasma bubbles and spread-F backscatter, we have plotted the backscatter profiles from beam positions 5 through 8 together with their corresponding electron density

profiles, in Figure 4. The backscatter from plume FAI is seen to have two maxima in all four profiles, suggesting a relationship to the internal structure of the plasma depletions.

As plotted, the backscatter maxima tend to occur at altitudes corresponding either to the electron density minima or the upper walls of the plasma depletions. If we allow for the 15-km altitude correction based on extrapolation along magnetic field lines, the backscatter maxima would appear to be associated with the upper walls of the plasma depletions. However, without knowledge of the vertical transport velocity, it is difficult to conclude what the exact spatial relationship is between radar backscatter maxima and plasma depletions.

Although vertical transport, in particular, that due to an upward bubble velocity, could drastically change the derived spatial relationship between radar backscatter and the plasma depletion, the backscatter profiles in Figure 4 can be used to argue that the backscatter cannot be grossly displaced with respect to the plasma depletions. Tsunoda et al. (1979) showed that IS measurements can be made even when the radar beam is directed perpendicular to the magnetic field, provided that spread-F backscatter is absent. Therefore, if a plasma depletion existed, without spatially-coincident spread-F backscatter, the depletion should be evident in the backscatter profiles in Figure 4. It is clear from examining these profiles that the depletions are not significantly displaced with respect to the backscatter region. From this observation, we conclude that the upward bubble velocity must have been negligibly small and did not distort the spatial relationship between spread-F backscatter and plasma depletions.

To lend further credence to the results just described, let us examine other electron density profiles obtained with the radar beam fixed at 10° south (geomagnetic) of vertical. In Figure 5, we show two electron density profiles taken shortly after the previous data set. On the basis of the assumed 100 m/s eastward drift speed, these profiles would correspond to features seen in Figure 2 that are located about 100 km west of ALTAIR. Both profiles show a plasma depletion at altitudes below 400 km, altitudes that seem to correspond to the leading edge of the 20-dB contour in Figure 2. Above the depletions, the profiles extend to altitudes above 600 km.

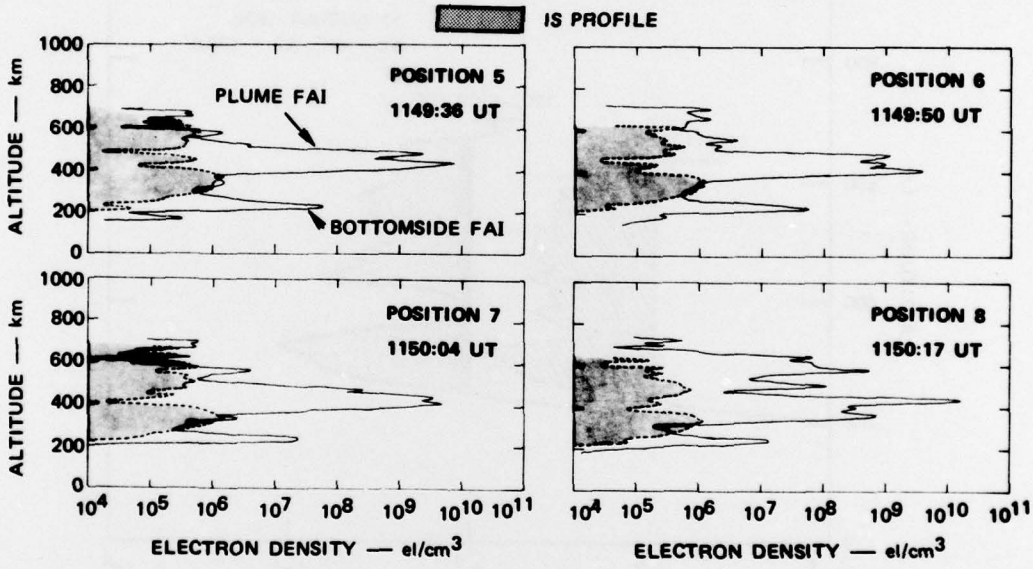

FIGURE 4 A COMPARISON OF PLUME BACKSCATTER PROFILES (solid curves) AND CORRESPONDING ELECTRON DENSITY PROFILES (dashed curves)

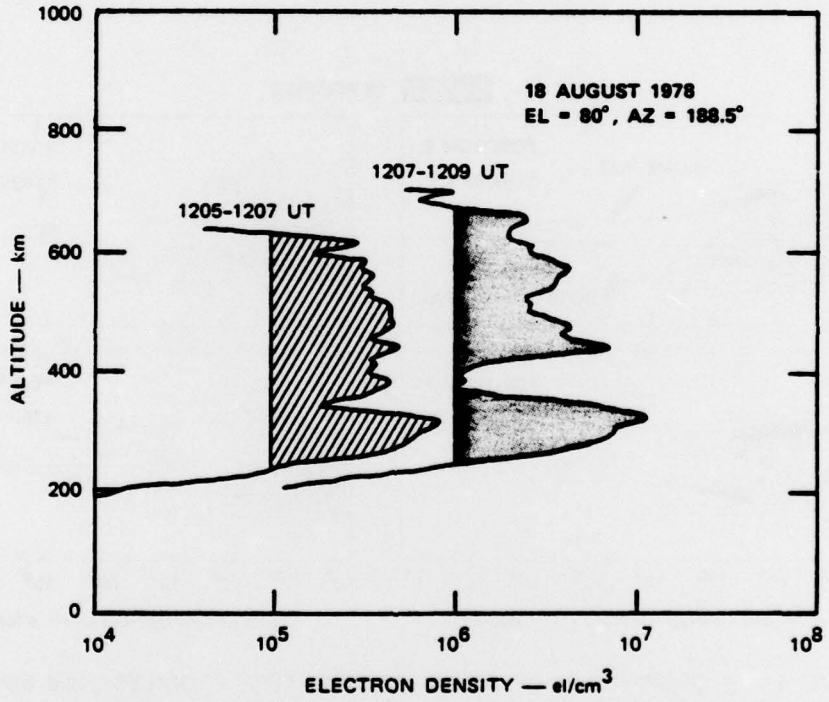

FIGURE 5 ELECTRON-DENSITY PROFILES OBTAINED ON 18 AUGUST 1978 WITH RADAR BEAM FIXED AT 10° SOUTH (geomagnetic) OF VERTICAL

The two profiles in Figure 5 can be compared to another pair of electron-density profiles, shown in Figure 6, taken at the same time on the following night when spread-F activity was much weaker. The profiles in Figure 6 display a peak electron density that appears to be somewhat higher than those in Figure 5, although the depletions (which occurred very close to the altitude of the F-layer peak) obscure the true peak electron density. The layer thickness of the F layer on both nights was comparable, with the layer extending from 250 to 650 km in altitude. The only noticeable difference in the background profiles is the slope of the topside of the F layer, being steeper on the quieter night.

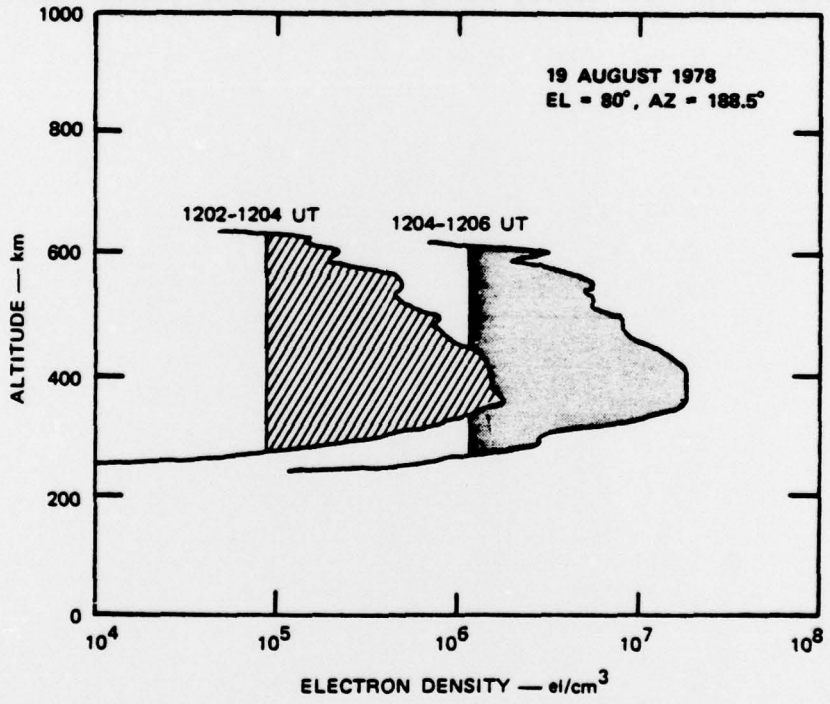

FIGURE 6 ELECTRON-DENSITY PROFILES OBTAINED ON 19 AUGUST 1978 WITH RADAR BEAM FIXED AT 10° SOUTH (geomagnetic) OF VERTICAL

IV DISCUSSION AND CONCLUSIONS

The results presented in this paper are some of the first on the two-dimensional spatial mapping of altitude-extended plasma bubbles. (Similar results have been reported by Towle [1979].) In-situ satellite measurements (Hanson and Sanatani, 1973; McClure et al., 1977) have all been longitudinal cuts through plasma bubbles. Plasma bubbles penetrated by rockets (Kelley et al., 1976; Morse et al., 1977) have all been no more than 10-20 km in altitude extent with depletions of approximately 50%.

The plasma bubbles presented in this paper extended over 100 km in both altitude and longitude, and had percentage plasma depletions approaching 99%. The factor that probably limits the highest percentage depletion that can be measured is the antenna sidelobes. Our estimate of -50-dB effective sidelobe gain appears to be confirmed by the data in Figure 4. The maximum separation between minima in plasma depletions and maxima in backscatter strength is no more than 50 dB.

The comparison of 1-m FAI distribution with the electron density profiles associated with plasma bubbles revealed a direct spatial relationship. Backscatter was found (1) to occur at the same altitude and (2) to have similar altitude extent as plasma depleted regions. Two maxima in backscatter strength were found to correspond with two minima in electron density. The only uncertainty is whether the backscatter is associated with the walls of the plasma bubbles or whether it occurs throughout the entire bubble volume. Because both backscatter and plasma depletions have comparable altitude extents, it is unlikely that radar backscatter is always confined to steep gradients associated with the walls of the plasma bubbles. Plasma structure must also exist within the bubble volume that is capable of producing significant backscatter.

The electron density profiles shown in Figure 5 suggest that a plasma depletion is not only associated with the "head" of the radar backscatter plume (i.e., the most intense portion of the backscatter

region that usually appears at high altitudes) but also with the "neck" of the radar plume (i.e., the portion that connects the plume head to the bottomside of the F layer). This conclusion supports the correctness of the collisional Rayleigh-Taylor instability model as the principal source mechanism of plasma bubbles (e.g., Ossakow and Chaturvedi, 1978).

REFERENCES

Hanson, W. B. and S. Sanatani, "Large Ni Gradients Below the Equatorial-F Peak," J. Geophys. Res., 78, 1167, 1973.

Kelley, M. C., G. Haerendel, H. Kappler, A. Valenzuela, B. B. Balsley, D. A. Carter, W. L. Ecklund, C. W. Carlson, B. Hausler, and R. Torbert, "Evidence for a Rayleigh-Taylor Type Instability and Upwelling of Depleted Density Regions During Equatorial Spread F," Geophys. Res. Letts., 3, 448, 1976.

McClure, J. P., W. B. Hanson, and J. H. Hoffman, "Plasma Bubbles and Irregularities in the Equatorial Ionosphere," J. Geophys. Res., 82, 2650, 1977.

Morse, F. A., B. C. Edgar, H. C. Koons, C. J. Rice, W. J. Heikkila, J. H. Hoffman, B. A. Tinsley, J. D. Winningham, A. B. Christiansen, R. F. Woodman, J. Pomalaza, and N. R. Teixeira, "Equion, an Equatorial Ionospheric Irregularity Experiment," J. Geophys. Res., 82, 578, 1977.

Ossakow, S. L. and P. K. Chaturvedi, "Morphological Studies of Rising Equatorial Spread-F Bubbles," J. Geophys. Res., 83, 2085, 1978.

Towle, D. M., "VHF and UHF Radar Observations of Equatorial Ionospheric Irregularities and Background Densities," submitted to Radio Science, 1979.

Tsunoda, R. T. and D. M. Towle, "On the Spatial Relationship of 1-Meter Equatorial Spread-F Irregularities and Depletions in Total Electron Content," submitted to Geophys. Res. Letts., 1979.

Tsunoda, R. T., M. J. Baron, J. Owen, and D. M. Towle, "ALTAIR: An Incoherent-Scatter Radar for Equatorial Spread-F Studies," submitted to Radio Science, 1979.

Woodman, R. F., "East-West Ionospheric Drifts at the Magnetic Equator," Space Res. XII, 12, 969, 1972.

Woodman, R. F. and C. La Hoz, "Radar Observations of F-Region Equatorial Irregularities," J. Geophys. Res., 81, 5447, 1976.

DISTRIBUTION LIST

DEPARTMENT OF DEFENSE

Assistant Secretary of Defense
Comm, Cmd, Cont & Intell
ATTN: Dir of Intelligence Systems, J. Babcock
ATTN: C3IST&CCS, M. Epstein

Assistant to the Secretary of Defense
Atomic Energy
ATTN: Executive Assistant

Command & Control Technical Center
ATTN: C-650, G. Jones
ATTN: C-312, R. Mason
3 cy ATTN: C-650, W. Heidig

Defense Advanced Rsch. Proj. Agency
ATTN: TIO

Defense Communications Agency
ATTN: Code R1033, M. Raffensperger
ATTN: Code 101B
ATTN: Code 205
ATTN: Code 480
ATTN: Code 810, J. Barna

Defense Communications Engineer Center
ATTN: Code R720, J. Worthington
ATTN: Code R123
ATTN: Code R410, J. McLean

Defense Technical Information
12 cy ATTN: DD

Defense Intelligence Agency
ATTN: DC-7D, W. Wittig
ATTN: DB, A. Wise
ATTN: DB-4C, E. O'Farrell
ATTN: HQ-TR, J. Stewart
ATTN: DT-1B
ATTN: DT-5

Defense Nuclear Agency
ATTN: STVL
ATTN: DDST
4 cy ATTN: TITL
3 cy ATTN: RAAE

Field Command
Defense Nuclear Agency
ATTN: FCPR

Field Command
Defense Nuclear Agency
Livermore Division
ATTN: FCPRL

Interservice Nuclear Weapons School
ATTN: TTV

Joint Chiefs of Staff
ATTN: J-37
ATTN: J-3, WWMCCS Evaluation Office
ATTN: C3S

DEPARTMENT OF DEFENSE (Continued)

Joint Strat Tgt Planning Staff
ATTN: JLTW-2
ATTN: JPST, G. Goetz

National Security Agency
ATTN: B-3, F. Leonard
ATTN: R-52, J. Skillman
ATTN: W-32, O. Bartlett

Undersecretary of Def for Rsch & Engrg
ATTN: Strategic & Space Systems (OS)

WWMCCS System Engineering Org.
ATTN: R. Crawford

DEPARTMENT OF THE ARMY

Assistant Chief of Staff for Automation & Comm.
Department of the Army
ATTN: DAAC-ZT, P. Kenny

Atmospheric Sciences Laboratory
U.S. Army Electronics R & D Command
ATTN: DELAS-EO, F. Niles

BMD Systems Command
Department of the Army
2 cy ATTN: BMDSC-HW

Deputy Chief of Staff for Ops & Plans
Department of the Army
ATTN: DAMO-RQC

Electronics Tech & Devices Lab
U.S. Army Electronics R & D Command
ATTN: DELET-ER, H. Bomke

Harry Diamond Laboratories
Department of the Army
ATTN: DELHD-N-P
ATTN: DELHD-I-TL, M. Weiner
ATTN: DELHD-N-P, F. Wimenitz
ATTN: DELHD-N-RB, R. Williams

U.S. Army Comm-Elec Engrg Instal Agency
ATTN: CCC-CED-CCO, W. Neuendorf
ATTN: CCC-EMEO, W. Nair
ATTN: CCC-EMEO-PED, G. Lane

U.S. Army Communications Command
ATTN: CC-OPS-W
ATTN: CC-OPS-WR, H. Wilson

U.S. Army Communications R&D Command
ATTN: DRDCO-COM-RY, W. Kesselman

U.S. Army Foreign Science & Tech Ctr
ATTN: DRXST-SD

U.S. Army Materiel Dev & Readiness Cmd
ATTN: DRCLDC, J. Bender

DEPARTMENT OF THE ARMY (Continued)

U.S. Army Nuclear & Chemical Agency
ATTN: Library

U.S. Army Satellite Comm Agency
ATTN: Document Control

U.S. Army TRADOC Systems Analysis Activity
ATTN: ATAA-TCC
ATTN: ATAA-PL
ATTN: ATAA-TCC, F. Payan, Jr.

DEPARTMENT OF THE NAVY

Joint Cruise Missile Project Office
Department of the Navy
ATTN: JCM-G-70

Naval Air Development Center
ATTN: Code 6091, M. Setz

Naval Air Systems Command
ATTN: PMA 271

Naval Electronic Systems Command
ATTN: PME 106-4, S. Kearney
ATTN: Code 3101, T. Hughes
ATTN: Code 501A
ATTN: PME 117-20
ATTN: PME 106-13, T. Griffin
ATTN: PME-117-2013, G. Burnhart
ATTN: 117-211, B. Kruger

Naval Intelligence Support Ctr
ATTN: NISC-50

Naval Ocean Systems Center
ATTN: Code 8151, C. Baggett
ATTN: Code 532, J. Bickel
ATTN: Code 5322, M. Paulson
3 cy ATTN: Code 5324, W. Moler

Naval Research Laboratory
ATTN: Code 6701, J. Brown
ATTN: Code 7580
ATTN: Code 6707, J. Davis
ATTN: Code 7500, B. Wald
ATTN: Code 6700, T. Coffey
ATTN: Code 7555

Naval Space Surveillance System
ATTN: J. Burton

Officer In Charge
Naval Surface Weapons Center
ATTN: Code F31

Naval Surface Weapons Center
ATTN: Code F-14, R. Butler

Naval Telecommunications Command
ATTN: Code 341

Office of Naval Research
ATTN: Code 420
ATTN: Code 421

Office of the Chief of Naval Operations
ATTN: OP 604C
ATTN: OP 941D
ATTN: OP 981N

DEPARTMENT OF THE NAVY (Continued)

Strategic Systems Project Office
Department of the Navy
ATTN: NSP-2141
ATTN: NSP-2722, F. Wimberly
ATTN: NSP-43, Tech. Library

DEPARTMENT OF THE AIR FORCE

Aerospace Defense Command/DC
Department of the Air Force
ATTN: DC, T. Long

Aerospace Defense Command/XPD
Department of the Air Force
ATTN: XP
ATTN: XPDQ

Air Force Avionics Laboratory
ATTN: AAD, W. Hunt
ATTN: AAD, A. Johnson

Air Force Geophysics Laboratory
ATTN: PHI, J. Euchau
ATTN: OPR-1, J. Ulwick
ATTN: PHP, J. Aarons
ATTN: LKB, K. Champion
ATTN: OPR, A. Stair
ATTN: PHP, J. Mullen

Air Force Weapons Laboratory
Air Force Systems Command
ATTN: SUL
ATTN: DYC

Air Logistics Command
Department of the Air Force
ATTN: OO-ALC/MM, R. Blackburn

Assistant Chief of Staff
Intelligence
Department of the Air Force
ATTN: INED

Assistant Chief of Staff
Studies & Analyses
Department of the Air Force
ATTN: AF/SASC, G. Zank
ATTN: AF/SASC, W. Adams

Deputy Chief of Staff
Operations Plans and Readiness
Department of the Air Force
ATTN: AFXOXFD
ATTN: AFXOKS
ATTN: AFXOKT
ATTN: AFXOKCD

Deputy Chief of Staff
Research, Development, & Acq.
Department of the Air Force
ATTN: AFRDS
ATTN: AFRDSP
ATTN: AFRDQ
ATTN: AFRDSS

Headquarters
Electronic Systems Division/DC
ATTN: DCKC, J. Clark

DEPARTMENT OF THE AIR FORCE (Continued)

Headquarters
Electronic Systems Division/XR
ATTN: XRW, J. Deas

Electronic Systems Division/YS
ATTN: YSEA
ATTN: YSM, J. Kobelski

Foreign Technology Division
Air Force Systems Command
ATTN: NIIS Library
ATTN: SDEC, A. Oakes
ATTN: TQTD, B. Ballard

Rome Air Development Center
Air Force Systems Command
ATTN: CCS, V. Coyne
ATTN: TSLD

Rome Air Development Center
Air Force Systems Command
ATTN: EEP

Ballistic Missile Office
Air Force Systems Command
ATTN: MNNL, S. Kennedy
ATTN: MNNH

Headquarters Space Division
Air Force Systems Command
ATTN: SKA, M. Clavin
ATTN: SKA, C. Rightmyer

Headquarters Space Division
Air Force Systems Command
ATTN: SZJ, L. Doan

Strategic Air Command
Department of the Air Force
ATTN: DCXF
ATTN: OOKSN
ATTN: DCX
ATTN: DCXT
ATTN: NRT
ATTN: DCXT, T. Jorgensen
ATTN: XPFS

DEPARTMENT OF ENERGY CONTRACTORS

Lawrence Livermore Laboratory
ATTN: Document Control for Technical Information Dept., Library

Los Alamos Scientific Laboratory
ATTN: Document Control for D. Westervelt
ATTN: Document Control for R. Taschek
ATTN: Document Control for P. Keaton

Sandia Laboratories
ATTN: Document Control for Org. 1250, W. Brown
ATTN: Document Control for D. Thornbrough
ATTN: Document Control for D. Dahlgren
ATTN: Document Control for 3141
ATTN: Document Control for Space Projects Div.

Sandia Laboratories
Livermore Laboratory
ATTN: Document Control for B. Murphy
ATTN: Document Control for T. Cook

OTHER GOVERNMENT AGENCIES

Central Intelligence Agency
ATTN: OSI/PSTD

Department of Commerce
National Bureau of Standards
ATTN: R. Moore

Department of Commerce
National Oceanic & Atmospheric Admin.
Environmental Research Laboratories
ATTN: R. Grubb
ATTN: Aeronomy Lab, G. Reid

Institute for Telecommunications Sciences
National Telecommunications & Info Admin
ATTN: A. Jean
ATTN: D. Crombie
ATTN: L. Berry
ATTN: W. Utlaut

U.S. Coast Guard
Department of Transportation
ATTN: G-DOE-3/TP54, B. Romine

DEPARTMENT OF DEFENSE CONTRACTORS

Aerospace Corp.
ATTN: F. Morse
ATTN: R. Slaughter
ATTN: D. Olsen
ATTN: I. Garfunkel
ATTN: T. Salmi
ATTN: S. Bower
ATTN: N. Stockwell
ATTN: V. Josephson

University of Alaska
Geophysical Institute
ATTN: N. Brown
ATTN: Technical Library
ATTN: T. Davis

Analytical Systems Engineering Corp.
ATTN: Radio Sciences

Analytical Systems Engineering Corp.
ATTN: Security

Barry Research Communications
ATTN: J. McLaughlin

BDM Corp.
ATTN: T. Neighbors
ATTN: L. Jacobs

Berkeley Research Associates, Inc.
ATTN: J. Workman

Boeing Co.
ATTN: G. Hall
ATTN: S. Tashird
ATTN: J. Kenney
ATTN: D. Murray

University of California at San Diego
ATTN: H. Booker

Computer Sciences Corp.
ATTN: H. Blank

DEPARTMENT OF DEFENSE CONTRACTORS (Continued)

Charles Stark Draper Lab, Inc.
ATTN: J. Gilmore
ATTN: D. Cox

COMSAT Labs
ATTN: G. Hyde
ATTN: R. Taur

Cornell University
Department of Electrical Engineering
ATTN: D. Farley, Jr.

EG&G, Inc.
ATTN: Document Control for D. Wright
ATTN: Document Control for J. Colvin

Electrospace Systems, Inc.
ATTN: H. Logston

ESL, Inc.
ATTN: C. Prettie
ATTN: J. Roberts
ATTN: J. Marshall

Ford Aerospace & Communications Corp.
ATTN: J. Mattingley

General Electric Co.
Space Division
ATTN: M. Bortner

General Electric Co.
Re-Entry & Environmental Systems Div.
ATTN: C. Zierdt
ATTN: S. Lipson
ATTN: A. Steinmayer

General Electric Co.
ATTN: F. Reibert

General Electric Company-TEMPO
ATTN: DASIAC
ATTN: D. Chandler
ATTN: M. Stanton
ATTN: T. Stevens
ATTN: W. Knapp

General Electric Tech Services Co., Inc.
ATTN: G. Millman

General Research Corp.
ATTN: J. Ise, Jr.
ATTN: J. Garbarino

GTE Sylvania, Inc.
Electronics Systems Group-Eastern Division
ATTN: M. Cross

HSS, Inc.
ATTN: D. Hansen

IBM Corp.
Federal Systems Division
ATTN: F. Ricci

University of Illinois
ATTN: K. Yeh

DEPARTMENT OF DEFENSE CONTRACTORS (Continued)

Institute for Defense Analyses
ATTN: E. Bauer
ATTN: J. Bengston
ATTN: H. Wolfhard
ATTN: J. Aein

International Tel & Telegraph Corp.
ATTN: G. Wetmore
ATTN: Technical Library

JAYCOR
ATTN: S. Goldman

JAYCOR
ATTN: D. Carlos

Johns Hopkins University
Applied Physics Lab
ATTN: T. Evans
ATTN: J. Newland
ATTN: Document Librarian
ATTN: T. Potemra
ATTN: P. Komiske
ATTN: B. Wise

Kaman Sciences Corp.
ATTN: T. Meagher

Linkabit Corp.
ATTN: I. Jacobs

Litton Systems, Inc.
AMECOM Division
ATTN: R. Grasty

Lockheed Missiles & Space Co., Inc.
ATTN: D. Churchill
ATTN: Dept. 60-12

Lockheed Missiles and Space Co., Inc.
ATTN: W. Imhof
ATTN: M. Walt
ATTN: R. Johnson

M.I.T. Lincoln Lab
ATTN: D. Towle
ATTN: L. Loughlin

McDonnell Douglas Corp.
ATTN: G. Mroz
ATTN: W. Olson
ATTN: J. Moule
ATTN: N. Harris

Mission Research Corp.
ATTN: S. Gutsche
ATTN: R. Hendrick
ATTN: M. Scheibe
ATTN: D. Sowle
ATTN: F. Fajen
ATTN: R. Bogusch

Mitre Corp.
ATTN: A. Kymmel
ATTN: C. Callahan
ATTN: G. Harding

DEPARTMENT OF DEFENSE CONTRACTORS (Continued)

Mitre Corp.
ATTN: W. Foster
ATTN: M. Horrocks
ATTN: W. Hall

Pacific-Sierra Research Corp.
ATTN: E. Field, Jr.

Pennsylvania State University
Ionosphere Research Lab
ATTN: Ionospheric Research Lab

Photometrics, Inc.
ATTN: I. Kofsky

Physical Dynamics, Inc.
ATTN: E. Fremouw

R & D Associates
ATTN: W. Karzas
ATTN: W. Wright, Jr.
ATTN: C. Greifinger
ATTN: C. MacDonald
ATTN: R. Lelevier
ATTN: F. Gilmore
ATTN: M. Gantsweg
ATTN: H. Ory
ATTN: R. Turco
ATTN: B. Gabbard

R & D Associates
ATTN: L. Delaney

Rand Corp.
ATTN: E. Bedrozian
ATTN: C. Crain

Riverside Research Institute
ATTN: V. Trapani

Rockwell International Corp.
Collins Telecommunications Sys. Division
ATTN: J. Kristof

Visidyne, Inc.
ATTN: J. Carpenter

DEPARTMENT OF DEFENSE CONTRACTORS (Continued)

Santa Fe Corp.
ATTN: E. Ortlieb

Science Applications, Inc.
ATTN: D. Hamlin
ATTN: J. McDougall
ATTN: D. Sachs
ATTN: L. Linson
ATTN: E. Straker
ATTN: C. Smith

Science Applications, Inc.
ATTN: D. Divis

Science Applications, Inc.
ATTN: SZ

SRI International
ATTN: R. Leadabrand
ATTN: W. Jaye
ATTN: G. Price
ATTN: W. Chesnut
ATTN: G. Smith
ATTN: R. Livingston
ATTN: C. Rino
ATTN: M. Baron
ATTN: A. Burns
ATTN: D. Neilson
ATTN: R. Tsunoda

Teledyne Brown Engineering
ATTN: R. Deliberis

Tri-Com, Inc.
ATTN: D. Murray

TRW Defense & Space Sys. Group
ATTN: D. Dee
ATTN: R. Plebuch
ATTN: S. Altschuler

Utah State University
Space Measurements Lab
ATTN: L. Jensen
ATTN: K. Baker